A Closed Loop between Microgeometry and BRDF for Wave Optics

ZIWEN YE, Carnegie Mellon University, USA

Given a material prototype whose visual appearance is determined by micro-scale details of its surface geometry, it's tempting to fabricate this appearance in any arbitrary shape. In this report, we investigate a closed loop between microgeometry in surface heightfields and the corresponding BRDFs for wave optics. We presented both derivations of BRDF from microgeometry, and vice versa using both geometric and wave optics methods.

Additional Key Words and Phrases: Computer Graphics, Wave Optics, Microfacet models, spatially-variant anisotropic BRDF

ACM Reference Format:
Ziwen Ye. 2020. A Closed Loop between Microgeometry and BRDF for Wave Optics. *ACM Trans. Graph.* 1, 1 (November 2020), 6 pages. https://doi.org/10.1145/nnnnnnn.nnnnnnn

1 INTRODUCTION

Novel materials fabricated in lab space are of small scales and possess complex surface geometry. These properties make them difficult to measure and simulate to produce realistic rendering results.

Realistic Rendering of novel materials is important for car industry. In car advertisements, they want to realistically recreate metal paints on the cars to match with their own appearance in real life. Being able to measure and render a material prototype allows preview of their products. Another potential application is for scientists to visualize their results in a virtual environment and have better analysis for their work

An established surface reflectance model is based on microfacet theory which states that the overall BRDF of the object can be modeled based on an arrangement of infinitesimally small facets.

But The way a surface reflects light is represented by its bidirectional reflectance distribution function (BRDF). The shape of a microfacet BRDF is primarily determined by the distribution of micro-scale surface normals, which is represented as a normal distribution function (NDF). Traditionally, simple distributions based on statistical assumptions about the surface, such as the Beckmann distribution, are used so that the parameters can be obtained by fitting to a relatively sparse set of BRDF measurements.[Walter et al. 2007; Zhao et al. 2014]

One approach in the past captured normal distribution by measuring microscopic surface topography. A profilometer that uses white-light interferometry through a microscope was used to measure the height fields, and measurements were done at high resolution regions at micron scales. With these measurements, they predicted accurate BRDF from the geometric surface normals. This method successfully captures BRDF information with easy setup and little time, but their method only examined known metal materials such as stainless steel, aluminum, and copper.[Zhao et al. 2014]

The article explores both the realm of high resolution rendering and geometry fabrication, which we hope to form a closed loop between the two variables : surface microgeometry and BRDF. We first discusses derivation of BRDFs from measured heightfields using both geometric and wave optics methods. Alternatively, we discuss fabrication of surface height fields from BRDFs using milling process. The ultimate goal of this article is to acquire and fabricate accurate, high resolution physical surfaces based on real measurements of material prototype in micron-scale.

2 RELATED WORKS

2.1 Microfacet BRDF

Microfacet theory is a geometric optics model which represents a material as an arrangement of infinitesimally small specular facets. It has been shown to be efficient in reproducing the behavior of a wide range of real materials.[Dupuy and Jakob 2018] The resulting BRDF thus have three terms, the microfacet Normal Distribution Function, a Fresnel term based on the material's complex index of refraction, and a shadow-masking term to ensure energy conservation. Out of the three terms, the most important is NDF since it is used to determine the pattern of reflected light. Many different parametric forms have been proposed to account for NDF. To model anisotropies of materials, Ward [Ward 1992] applied the anisotropic Beckmann distribution, which ignored the Fresnel and the shadowing masking term for simplicity. Walter [Walter et al. 2007] introduced the GGX distribution which is better suited to modelling spatial variations in materials.

Microfacet theory assumes the diffraction effects can be ignored using geometric optics. But such an assumption holds only when micro-surfaces are locally flat compared to the wavelength. In reality, material surfaces break this assumption. The above methods has not addressed their limits to the actual microgeometry of surfaces. Zhao [Zhao et al. 2014] measured surface geometry and developed a modified NDF estimation in a geometric optics context to accurately predict BRDFs for anisotropic materials.

2.2 Modeling Microgeometry

Zhao [Zhao et al. 2014] used X-ray computed tomography (CT) to measure the 3D structure of a small area of the cloth and acquire a volumetric model. They use multiple CT images to reconstruct density and orientation fields, then use optical parameters of the volumetric model to pattern match across the whole cloth to generate highly realistic results. Dong [Dong et al. 2015] measured surface

Author's address: Ziwen Ye, Carnegie Mellon University, 5032 Forbes Ave, Pittsrbugh, PA, 15213, USA, ziweny@andrew.cmu.edu.

0730-0301/2020/11-ART $15.00
https://doi.org/10.1145/nnnnnnn.nnnnnnn

microgeometry of metals using a profilometer which is generally found in photolithography and nanofabrication. Using a profilometer allows rapid BRDF acquisition with both high spatial and angular resolution, but it only predicts the first surface reflection for the surfaces. CT imaging, though slow in speed, captures the full 3D volumetric information and is suitable for complex, thick materials like textiles. Yan [Yan et al. 2014] captures the true normal distributions on a surface patch seen through a pixel.

2.3 Material Fabrication

Dong [Dong et al. 2010] presented a method for fabricating a material volume with a desired BSSRDF(bidirectional subsurface scattering reflectance distribution function). Optically thick materials whose subsurface scattering behavior is captured by diffusion approximation are stacked with varying thickness and composition and reproduce a wide variety of heterogeneous BSSRDFs. Hašan [Hašan et al. 2010] proposed a different pipeline process which produces both homogeneous and heterogeneous composites with a multi-material 3D printer instead of a milling machine and a 3D printed color texture as proposed by Dong et al [2010] Rouiller [Rouiller et al. 2013] uses analytic NDF as input to optimize a microgeometry that reproduces a normal distribution corresponds to the desired NDF, allowing fabrication ofspatially varying BRDFs (svBRDFs) on 3D models.

2.4 Fabricating Microgeometry

Weyrich [2009] proposed a system for manufacturing physical surfaces given a user-specified BRDF using milling machines. The derived surface height field has high angular resolution, but the spatial resolution is limited. Levin et al. [2013]incorporated wave optics into fabrication design, and fabricated spatially varying BRDF using photolithogrphay, improving spatial resolution up to 220 dpi (dots per inches). Alternatively, Schwartzburg et al [2014] presented an algorithm for inverse caustic design by integrating adaptive Voronoi discretization scheme. Their methods enabled high-contrast target images.

3 METHODS

Our goal is to reproduce complex surface appearances in high spatial resolution for material surfaces given information about height fields. In addition, we hope to fabricate heightfields given existing BRDFs, forming a closed loop between the two variables. Given the limits of access to optical profilometer, we use prior height field data to reconstruct BRDF based on the following methods. Using microfacet theory to predict normal distribution function (NDF)as the primary determinant of a BRDF's shape. An alternative method is based on approximating the micron-resolution surface wave effects using Gabor kernels(products of Gaussians with complex exponentials). In section 4, we will first discuss wave optics theory. Section 5 describes microfacet theory. section 6 will introduce efficient BRDF evaluation using Gabor kernels. Section 7 touches on the derivation of heightfield from BRDF.

Diffraction BRDF model	ξ_1	ξ_2	ξ_3
Kirchhoff	$\frac{\lvert\psi\cdot n\rvert^2 F}{4\lambda^2\lvert\omega_i\cdot n\rvert\lvert\omega_o\cdot n\rvert}$	$1-\frac{\psi\cdot\bar{H}'(s)}{\psi\cdot n}$	$\psi\cdot n$

Table 1. List of symbols

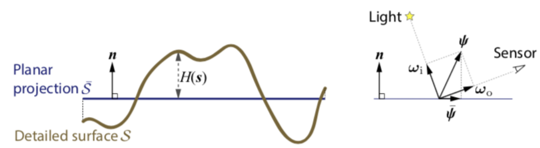

Fig. 1. Heightfield surface and BRDF directions example. [2014]

4 WAVE BRDF THOERY

In wave optics, light is considered as wave that satisfy certain boundary conditions and governing differential equations. Each wavelength (denoted as λ) is considered individually and encoded by magnitude and phase using complex-valued fields. The local light energy is characterized as squared magnitude of the field as that point. Certain scalar diffraction models, including Kirchhoff theory, can be used to estimate the reflected field from a rough surface. Unlike geometry optics, wave optics can result in characteristic diffraction effects, attributing from non-linear sum due to interference effects. [2014]

Given a surface heightfield $H(s)$(seen Table 1) for a 2D point, $s = [s_x, s_y]$, we have a corresponding 3D point on the rough surface denoted as $[s_x, s_y, H(s)]$. Here, we are discretizing heightfield into texel of $1\mu m$ resolution, and our goal is to estimate the BRDF with these height information. Due to difference in local surface height, light reflecting from different parts of the surface will travel different distances. This causes phase shifts in reflected waves which can be described as interference to determine the BRDF.

These phase shifts can be approximated using a planar surface that reflects light with spatially-varying phase shift, specified by its reflection function[2014]:

$$R(s) = \xi_2 e^{-i\frac{2\pi}{\lambda}\xi_3 H(s)} \tag{1}$$

A typical diffraction models we use is Kirchhoff model with values of ξ_2 and ξ_3 specified in Table 2. Here, we represent directions ω_i and ω_o as 3D unit vectors. Let $\psi = \omega_i + \omega_o$ and $\bar{\psi}$ be its 2D projection on XY plane as seen in Table 2. The BRDF of this planar representation can be computed using a surface integral of the form:

$$f_r(\omega_i, \omega_o) = \frac{\xi_1}{A_{\bar{S}}} \left| \int_{\bar{S}} R(s) e^{-i\frac{2\pi}{\lambda}(\bar{\psi}\cdot s)} ds \right|^2 \tag{2}$$

where $\bar{S}$ is the domain of the heightfield, $A_{\bar{S}}$ is its area, and ξ_i depends on the chosen BRDF model.

4.1 Coherence area

Kirchhoff diffraction model simulates incident lights as coherent light wave, but in reality, the light sources from real scenes are

i	Imaginary unit for complex numbers,
λ	Wavelength of light
n	Average surface normal(equal to z axis)
s	2D point(on the XY plane)
$H(s)$	Height of surface above s
$\bar{S}$	domain of height function
$A_{\bar{s}}$	Area of $\bar{S}$
ω_i	Direction of incident light (3D unit vector)
ω_o	Direction of reflected light (3D unit vector)
ψ	$\psi = \omega_i + \omega_o$
$\bar{\psi}$	2D projection of ψ on XY plane
f_x	Bidirectional refelctance distribution function (BRDF)
F	surface reflectance
ξ_1, ξ_2, ξ_3	see Figure 2

Table 2. List of symbols

much more complicated, so an infinite coherence area as shown in equation 2 is impractical. Thus, we define the spatial area over which the phase of light remains coherent is called the coherence area. This areas is usually inversely correlated to the solid angle. For a simple uniform source, the coherence area is approximately given by $A_c \approx \lambda^2/\Omega_l$, where Ω_l is the solid angle subtended by light source in steradians [Mandel and Wolf 1995]. To account for the effect of coherence area, we spatially limit the surface integral using coherence kernels $w(s)$, and then take an average of the resulting BRDF over the region of interest. The principle effect of limiting the coherence area is the blurring of the BRDF. The BRDF estimation over one coherence area now becomes

$$f_r(\omega_i, \omega_o) = \frac{\xi_1}{A_c} \left| \int_{\bar{S}_c} R^*(s) e^{-i\frac{2\pi}{\lambda}(\bar{\psi}\cdot s)} ds \right|^2 \tag{3}$$

$$R^*(s) = w(s - x_c)R(s) \tag{4}$$

where $\bar{S_c}$ is the portion of $\bar{S}$ within the support of the coherence kernel centered at x_c, the corresponding normalization factor is $A_c = \int |w(s)|^2 ds$, and R^* is the product of $R(s)$ and the coherence kernel.[2014]. Generally, the actual coherence area depends of the details of the lighting configuration which is unknown in advance, so we can't predict the exact coherence area. Although overestimation and underestimation can cause problems such as high angular frequency aliasing and over-blurring of the BRDF, we can resolve this by capturing more light samples.

To simplify rendering procedure, we applied a fixed size coherence area over the entire region and use a Gaussian with standard deviations of 10 microns for w [Werner et al. 2017].

5 MICROFACET THEORY

Microfacet theory considers a surface as a collection of tiny flat mirror facets, that obey geometric optics. At each point, the surface reflects incident light to their corresponding mirror direction based on the local surface normal. So light coming from incident direction ω_i will only be reflected to out direction ω_o by facets on the surface whose normals are equal to ψ. The area density with a given local normal is describedby the surface's normal distribution function(NDF) [2014]. The BRDF function corresponding to the microfacet model is given by

$$f_r(\omega_i, \omega_o) = \frac{D_M(\psi)F(\omega_i, \psi)G(\omega_i, \omega_o)}{4|\omega_i \cdot n||\omega_o \cdot n|} \tag{5}$$

where D_M is the surface's normal distribution function, F is the Fresnel term, G is a shadowing-masking term, and n is the average of the normal. [2014]. The Fresnel term is determined by the material type and can be computed based on its reflectance index and extinction coefficients. The shadow-masking term is used for energy conservation and is typically close to one. So the most important function is the normal distribution function.

Traditional Microfacet theory neglects wave effects including diffraction, so it can't accurately capture the roughness at scales near the wavelength of light. To simulate BRDF results, [2014] devised a filtered geometric NDF estimation. A surface's normal distribution function (NDF) is a density function over the sphere of directions that is proportional to the surface area with a given surface normal m [2014]. The NDF can be defined geometrically as

$$D_M(m) = \lim_{|\omega_m| \to 0} \frac{A(\Omega_m)}{|\Omega_m| A_S^{\perp}}, \tag{6}$$

where Ω_m is a solid angle containing the direction m, $A(\Omega_m)$ is the area of surfaces whose normals are inside Ω_m, and $A_S^{\perp}$ is the total projected surface area in the direction of the large scale surface normal n.

To account for the effects of wave optics which surface details below wavelength-scale has much reduced influence on BRDF. We propose a modified NDF estimation that uses a Gaussian filter to reduce the influence of small scale features.

6 EFFICIENT BRDF EVALUATION

In this section, we would discuss approaches to efficiently evaluate the BRDF integrals for our wave optics diffraction models. One ideas is to approximate the phase-delay reflection function $R^*(s)$ by a weighted combination of *Gabor kernels*, which are products of a 2D Gaussian with a complex exponential (plane wave). These kernels contain desirable properties that represents high frequency features seen in $R^*(s)$

6.1 Gabor kernels

We define a Gabor kernel as the product of a 2D Gaussian and a complex exponential:

$$g(s; \mu; \sigma, a) = G_{2D}(s; \mu,)e^{-i2\pi(a\cdot s)} \tag{7}$$

where $G_{2D}(s; \mu, \sigma) = \frac{1}{2\pi\sigma^2} exo(-\frac{\|s-\mu\|^2}{2\sigma^2})$ is a normalized 2D Gaussian isotropic[Yan et al. 2014]. μ is the center, σ the width, and a the plane wave parameter.

6.2 Approximating R with Gabor kernels

Here, we adapted our approximation algorithm from Yan et al.[2014].We first subdivide our height field domain $\bar{S}$ into uniform grid of cells. The size of these cells should match the original height field texels. Next, we select a set of cells, whose centers are located at m_k that covers the current coherence kernel we are integrating over. We treat the coherence kernel over a cell as constant with value of $w_k = w(m_k - x_c)$[2014] since the area of the cell is much smaller than that of the coherence area. Then we place a Gabor kernel centered in each of the grid to approximate reflection function $R(s)$ in its neighbor, and this provides us with an approximation of the $R^*(s)$ expressed as :

$$R^*(s) \approx \sum_k w_k R_k(s) = \sum_k w_k C_k g(s; m_k, \sigma_k, a_k) \tag{8}$$

, where C_k is a complex constant, incorporating an appropriate scaling coefficient that incorporates both an appropriate scaling coefficient and phase shift.

We then approximate the heightfield $H(s)$ in each cell using first order expansion of m_k which results :

$$H(s) \approx H(m_k) + H'(m_k) \cdot (s - m_k) \tag{9}$$

$$= H'(m_k) \cdot s + (H(m_k) - H'(m_k) \cdot m_k) \tag{10}$$

where $H'(m_k)$ is the gradient of the heightfield at m_k. [2014]. Given this approximation, we now substitute this equation back to our original definition of $R(s)$ in equation 1, which we approximate the contribution of a single cell as

$$R_k(s) = B_{2D}(s; m_k, l_k)\xi_2 e^{-\frac{i2\pi\xi_3}{\lambda} H(s)} \tag{11}$$

$$\approx l_k^2 G_{2D}(s; \mu_k, \sigma_k)\xi_2 e^{-\frac{i2\pi\xi_3}{\lambda}(\alpha_k + H'(m_k)\cdot s)} \tag{12}$$

where $\alpha_k = H(m_k) - H'(m_k) \cdot m_k$ as the result of first order approximation. B_{2D} is a binary box function inferring the domain of the grid cell, which integrates to the cell's area l_k^2. Subsequently, we replace this box function with a 2D Gaussian function covering the same area. Lastly, by comparing the result from equation 12 to that of equation 8, we have

$$C_k = l_k^2 \xi_2 e^{-\frac{i2\pi\xi_3}{\lambda}(H(m_k) - H'(m_k \cdot m_k)} \tag{13}$$

$$a_k = \frac{\xi_3 H'(m_k)}{\lambda} \tag{14}$$

6.3 BRDF Approximation

Lastly, we can use the Gabor kernel approximation derived earlier to evaluate the BRDF. Using equation 5, we get

$$f_r(\omega_i, \omega_o) = \frac{\xi_1}{A_c} |\sum_k w_k C_k \mathcal{F}[g(s; m_l, \sigma_k, a_k)](\frac{\bar{\psi}}{\lambda})|^2 \tag{15}$$

,where the fourier transform is defined as

$$\mathcal{F}[f](v) \equiv \int_{\mathbb{R}^2} f(s) e^{-i2\pi(s\cdot v)} ds \tag{16}$$

7 FROM BRDF TO HEIGHTFIELD

7.1 BRDF to Microfacet Distribution

In order to form a close loop, we now seek for the inverse process, namely converting BRDFs to heightfields. Here, we adopt method presented by Weyrich et al.[2009] and introduce fabrication of microgeometry using a milling machine. Note that the derivation is different depending on the fabrication process we are using. For instance, photolithography prefers surfaces which are composed of a small number of piece-wise flat layers, while milling prefers continuous depth surface.[Levin et al. 2013; Weyrich et al. 2009]

We first represent BRDF as half-angle distribution, then we convert this distribution into the desired normal distribution function, by accounting the base BRDF. The effect of BRDF can be treated as a convolution. Removing the effect involves solving a deconvolution problem. Here, we use the iterative Lucy-Richardson deconvolution algorithm

7.2 Microfacet Distribution to Height Field

In principle, there may exist an infinite possibility of height field that produces the same microfacet distribution, but not every distribution describes a continuous tileable surface and can be fabricated. To constraint the problem, we need to satisfy the following constraint, which by rotating the microfacet distribution, its mean is perpendicular to the surface. Given this precondition, we devise a sampling method and optimization scheme to maximize tileability, and minimize discontinuities. Lastly, we solve for the optimal height of each facet.

Sampling A possible sampling method is to apply importance sampling. Since the order of the microfacets does not impact the distribution, using low-discrepancy sampling techniques will achieve great-fidelity while maintaining a low noise level. Since we have no direct control of the "brightness" over the microfacet distribution(light is reflected based onthe base BRDF which we eliminated in the previous step), we employ a centroidal Voronoi tessellation technique to place the sample proportional to the local density, while maintaining a good global distribution of the samples [2009].

Optimization Given the desired sets of microfacets we sample, we need to optimize our tiles to meet the necessary preconditions: a smooth, manufacturable surface. Here, we formulate this minimization problem as a combination of three heuristical energy functions. The first energy function $C = C_x + C_y$, penalizes slope incompatibility between adjacent facets in x and y direction:

$$C_x = \frac{1}{4} \sum_y \sum_x \| \frac{dz(x+1,y) - dz(x,y)}{dy} \|^2 \tag{17}$$

and C_y analogously.[2009]. This equation enforces neighboring facets have a similar slope along their common edges. Next, we enforce integrability along rows and columns by minimizing the second energy function $I = I_x + I_y$, ensuring that in a cyclic arrangement, the derivatives along each row or column sum to zero

$$I_x = \sum_y \| \sum_x \frac{dz(x+1,y) - dz(x,y)}{dx} \|^2 \tag{18}$$

,and I_y analogously [2009]. Lastly, since we are using milling machine, we need to account for the shape of milling bits. For instance, we cannot manufacture arbitrary concave shape since such a shape would introduces erroneous angles of reflection. To reduce this problem, we introduce the last term $V = V_x + V_y$ adds a constant penalty when two neighboring facets form a concave slope

$$V_x = w_v |(x,y)| \frac{dz(x+1,y)}{dx} > \frac{dz(x,y)}{dx}| \tag{19}$$

and V_y analogously, with w_v as a weighting term depending on the relative influence of concavity compared to other penalty functions [2009].

Integration Provided with the optimal 2D arrangement of the microfacets using the previous optimizations, we seek to optimize for maximal continuity in height field by shifting each facet along z direction to their optimal heights. We describe this problem as a discrete Possion equation

$$\nabla^2 z = \text{div} g \tag{20}$$

, with a gradient field $g = (g_x, g_y)$ and the condition for seamless facet connectivity in the direction being

$$g_x(x,y) = \frac{1}{4}\frac{dz(x-1,y)}{dx} + \frac{1}{2}\frac{dz(x,y)}{dx} + \frac{1}{4}\frac{dz(x+1,y)}{dx} \tag{21}$$

and g_y analogously. As we aim a tileable arrangement given a cyclic system, a Dirichlet boundary condition at a single point suffice to solve the equation.

8 RESULTS AND DISCUSSIONS

We adapted implementation of Gabor kernel solution from Yan et al.[2014], and tested on simulated isotropic and scratched height fields as well as height fields of aluminum captured using profilometer provided by zhao et al [2014]. The results we acquired from the isotropic and scratched heightfields are shown in Figure 2. As for the aluminum surface heightfields, we stitched several patches from the measured data to form an image of size 1024x1024 pixels, and ran the BRDF integration at a wavelength of 0.11 microns, similar to the size of each texel as reported by zhao et al [2014]. However, the derivation we received does not seem reasonable. On the other hand, we derived the NDF for Aluminum 4, copper 4, and Qpanel which is a steel plate with an isotropic rough finish using heightfields data from zhao et al [2014] and Kirchhoff diffraction model as shown in figure 3. Due to the time constraint, we didn't get to the other direction of the closed loop: fabricating microgeometry from BRDF. In the future, we would like to derive a heightfields and potentially manufacture these heightfields distribution using various methods such as photolithography and milling.

8.1 Conclusions

In this report, we presented ideas and methods to form a closed loop between heightfields and BRDFs using wave optics. We discussed derivation of BRDFs with measured heightfields in micron scale using either Gabor kernel or microfacet theory. In addition, we discussed methods for fabricating microgeometry from BRDFs, specifically using milling. In results, we showed the BRDF results with simulated isotropic and scratched heightfields, but couldn't get the results for real measurements. Alternatively, we presented the NDF results using Kirchhoff diffraction model for Aluminum 4, Copper 4, and Qpanel. We didn't obtain results of microgeometry from BRDF due to the time constraints, but we hope to achieve this in the future.

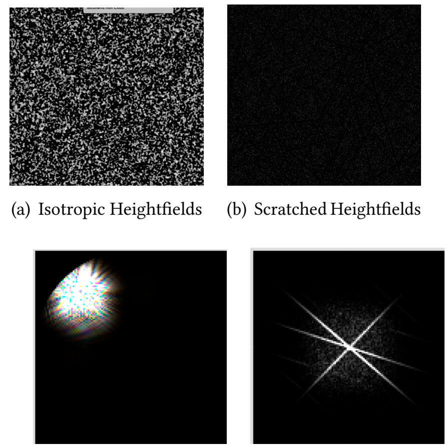

(a) Isotropic Heightfields (b) Scratched Heightfields

(c) Isotropic BRDF (d) Scratched BRDF

Fig. 2. The heightfields of different surfaces and their corresponding BRDFs

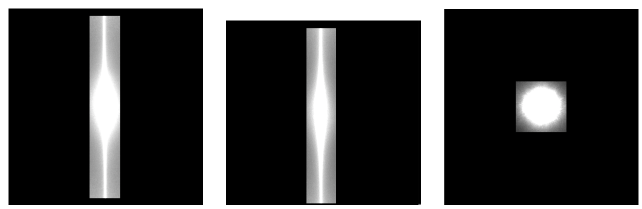

(a) Aluminum 4 (b) Copper4 (c) Qpanel

Fig. 3. The NDF of Aluminum 4, Copper 4, and Qpanel using Kirchhoff diffraction model

REFERENCES

Yue Dong, Jiaping Wang, Fabio Pellacini, Xin Tong, and Baining Guo. 2010. Fabricating Spatially-Varying Subsurface Scattering. In *ACM SIGGRAPH 2010 Papers (SIGGRAPH '10)*. Association for Computing Machinery, New York, NY, USA, Article Article 62, 10 pages. https://doi.org/10.1145/1833349.1778799

Zhao Dong, Bruce Walter, Steve Marschner, and Donald P Greenberg. 2015. Predicting Appearance from Measured Microgeometry of Metal Surfaces. *ACM Transactions on Graphics* 15, 1 (December 2015). https://doi.org/10.1145/2815618

Jonathan Dupuy and Wenzel Jakob. 2018. An Adaptive Parameterization for Efficient Material Acquisition and Rendering. *ACM Trans. Graph.* 37, 6, Article Article 274 (Dec. 2018), 14 pages. https://doi.org/10.1145/3272127.3275059

Miloš Hašan, Martin Fuchs, Wojciech Matusik, Hanspeter Pfister, and Szymon Rusinkiewicz. 2010. Physical Reproduction of Materials with Specified Subsurface Scattering. In *ACM SIGGRAPH 2010 Papers (SIGGRAPH '10)*. Association for Computing Machinery, New York, NY, USA, Article Article 61, 10 pages. https://doi.org/10.1145/1833349.1778798

Anat Levin, Daniel Glasner, Ying Xiong, Frédo Durand, William Freeman, Wojciech Matusik, and Todd Zickler. 2013. Fabricating BRDFs at High Spatial Resolution Using Wave Optics. *ACM Trans. Graph.* 32, 4, Article 144 (July 2013), 14 pages. https://doi.org/10.1145/2461912.2461981

Leonard Mandel and Emil Wolf. 1995. *Optical Coherence and Quantum Optics*. Cambridge University Press. https://doi.org/10.1017/CBO9781139644105

Olivier Rouiller, Bernd Bickel, Wojciech Matusik, Marc Alexa, and Jan Kautz. 2013. 3D-Printing Spatially Varying BRDFs. *IEEE Comput. Graph. Appl.* 33, 6 (Nov. 2013), 48–57. https://doi.org/10.1109/MCG.2013.82

Yuliy Schwartzburg, Romain Testuz, Andrea Tagliasacchi, and Mark Pauly. 2014. High-Contrast Computational Caustic Design. *ACM Trans. Graph.* 33, 4, Article 74 (July 2014), 11 pages. https://doi.org/10.1145/2601097.2601200

Bruce Walter, Stephen R. Marschner, Hongsong Li, and Kenneth E. Torrance. 2007. Microfacet Models for Refraction through Rough Surfaces. In *Proceedings of the 18th Eurographics Conference on Rendering Techniques (EGSR'07)*. Eurographics Association, Goslar, DEU, 195–206.

Gregory J. Ward. 1992. Measuring and Modeling Anisotropic Reflection. *SIGGRAPH Comput. Graph.* 26, 2 (July 1992), 265–272. https://doi.org/10.1145/142920.134078

Sebastian Werner, Zdravko Velinov, Wenzel Jakob, and Matthias B. Hullin. 2017. Scratch Iridescence: Wave-Optical Rendering of Diffractive Surface Structure. *ACM Trans. Graph.* 36, 6, Article 207 (Nov. 2017), 14 pages. https://doi.org/10.1145/3130800.3130840

Tim Weyrich, Pieter Peers, Wojciech Matusik, and Szymon Rusinkiewicz. 2009. Fabricating Microgeometry for Custom Surface Reflectance. *ACM Trans. Graph.* 28, 3, Article 32 (July 2009), 6 pages. https://doi.org/10.1145/1531326.1531338

Ling-Qi Yan, Miloš Hašan, Wenzel Jakob, Jason Lawrence, Steve Marschner, and Ravi Ramamoorthi. 2014. Rendering Glints on High-Resolution Normal-Mapped Specular Surfaces. *ACM Trans. Graph.* 33, 4, Article Article 116 (July 2014), 9 pages. https://doi.org/10.1145/2601097.2601155

Shuang Zhao, Wenzel Jakob, Steve Marschner, and Kavita Bala. 2014. Building Volumetric Appearance Models of Fabric Using Micro CT Imaging. *Commun. ACM* 57, 11 (Oct. 2014), 98–105. https://doi.org/10.1145/2670517